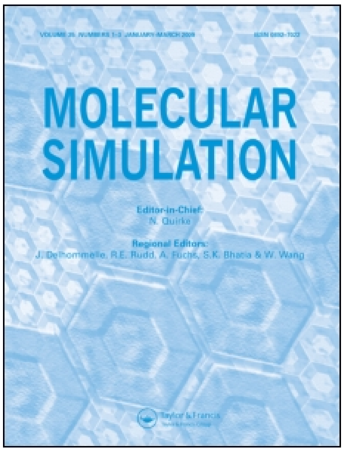

Molecular Simulation
Publication details, including instructions for authors and subscription information:
http://www.informaworld.com/smpp/title~content=t713644482

Properties of Confined Square-well Fluids using the Gibbs Ensemble Simulation Technique

Luis Alberto del Pino[a]; Ana Laura Benavides[a]; Alejandro Gil-Villegas[a]
[a] Instituto de Física, Universidad de Guanajuato, León, México

Online publication date: 26 October 2010

To cite this Article Pino, Luis Alberto del , Benavides, Ana Laura and Gil-Villegas, Alejandro(2003) 'Properties of Confined Square-well Fluids using the Gibbs Ensemble Simulation Technique', Molecular Simulation, 29: 6, 345 — 356
To link to this Article: DOI: 10.1080/0892702031000117199
URL: http://dx.doi.org/10.1080/0892702031000117199

Molecular Simulation, Vol. 29 (6–7), June 2003, pp. 345–356

Taylor & Francis
Taylor & Francis Group

Properties of Confined Square-well Fluids using the Gibbs Ensemble Simulation Technique

LUIS ALBERTO DEL PINO*, ANA LAURA BENAVIDES† and ALEJANDRO GIL-VILLEGAS

Instituto de Física, Universidad de Guanajuato, Apdo. Postal E-143, León, México

(Received April 2002; In final form August 2002)

In this work we have used the extension of the Gibbs ensemble simulation technique to inhomogeneous fluids [Panagiotopoulos, A.Z. (1987) "Adsorption and capillary condensation of fluid in cylindrical pores by Monte Carlo simulation in the Gibbs ensemble", *Mol. Phys.*, 62 (3), 701–719], which has been applied to adsorption phenomena of confined fluids. Fluid molecules are described by spherical particles interacting via a square-well potential. The fluid is confined in two types of walls: symmetrical (two hard walls) and non-symmetrical (one square-well wall and one hard wall). In order to analyze the behavior of the confined fluid by varying the potential parameters, we evaluated the bulk and confined densities, the internal energies and the density profiles for different supercritical temperatures. A variety of adsorption profiles can be obtained by using this model. The simulation data reported here complements the available simulation data for this system and can be useful in the development of inhomogeneous fluid theories. Since the square-well parameters can be related to real molecules this system can also be used to understand real adsorption systems.

Keywords: Confined fluid; Gibbs ensemble Monte Carlo simulation; Adsorption; Square-well potential; Competing interactions; Adsorption isotherms

INTRODUCTION

Membrane separation technologies, chromatography, oil recovery and catalysis are examples of phenomena that appear in confined fluids. An understanding of these systems is important in order to generate theoretical methods useful to the chemical engineers. Simple and complex inhomogeneous fluid models have been used to study the adsorption phenomena by theoretical and computer simulation methods [2–18]. For the case of simple confined fluids, different interparticle potentials (e.g. hard-sphere, Lennard–Jones, hard-sphere Yukawa and square-well (SW)) have been used in different confinement geometries and wall textures. These idealized systems are useful since their structural and thermodynamic properties have been extensively studied for homogeneous fluids, and then can be incorporated in theories for inhomogeneous fluids. The SW potential has three parameters (diameter, energy depth and range) that permits to model a great number of real substances, and several analytical equations of state have been proposed for this system using, for example, perturbation theory [19–23]. This model has been used previously to study the adsorption of SW molecules in a gas–liquid phase confined between symmetrical and non-symmetrical walls (a SW wall and a hard wall) [2,3,5,7,15,17,18] by density functional theory and molecular simulation. Special attention has been devoted to the wetting and drying transitions that appear with this simple model potential that is non-conformal due to the variable range parameter. These types of transitions have been observed also in experimental work [24]. Besides, adsorption of Noble gases on graphite has been accurately described by a theoretical approach that considers the system as a quasi two-dimensional monolayer formed by a SW system coexisting in equilibrium with a three dimensional SW bulk system [8].

The main purpose of this work is to study in a systematic way the behavior of a confined SW fluid when the parameters of the potentials that

*Facultad de Montaña, San Andrés, Universidad de Pinar del Río, Cuba.
†Corresponding author. E-mail: alb@ifug3.ugto.mx

ISSN 0892-7022 print/ISSN 1029-0435 online © 2003 Taylor & Francis Ltd
DOI: 10.1080/0892702031000117199

characterize the molecule–molecule and the molecule–wall interactions, the density and temperature are changed. This study could be useful in the design of real adsorption systems and to develop theories. We concentrate this study to supercritical temperatures in order to complement the data obtained by other authors [2,3,5,7,15,17] and also because we are interested in the behavior of the system when the bulk fluid is in one single phase. We have considered two types of walls: symmetrical (two hard walls) and non-symmetrical (a SW-type left wall and a right hard wall). We have selected the non-symmetrical case not only because similar walls were considered by other authors [3,17] in their molecular dynamics simulations, but also because we wanted to analyze the effect of competing walls. This situation could correspond to the limit of a scenario of a mixture of colloidal particles in a solution with a molecular fluid. The particles of the solvent can be considered as a confined fluid, being the colloidal particles the "walls" of the system. Competing walls mean here a molecular fluid attracted by one type of colloidal particles whereas there is repulsion with the other colloidal particles. Besides Parry and Evans have shown that non-symmetrical walls are responsible of a very interesting behavior near the critical point [25,26]. We expect that the results from the present work could also be useful in future work devoted to a more detailed analysis near the critical point. We have selected the Gibbs ensemble simulation technique for inhomogeneous fluids [1] since it is a very efficient method that provides structural and thermodynamic properties of bulk and confined systems for a given temperature. This advantage permitted a more complete analysis than using only the Monte Carlo NVT simulation technique [14].

In the second section we present the model potentials. The details of the simulation technique are given in the third section. In the fourth section we present the simulation data and the corresponding analysis. Finally, in the fifth section we give the conclusions of this work.

THE MOLECULE–MOLECULE AND MOLECULE–WALL POTENTIALS

We consider a fluid formed by N spherical particles interacting via a square-well potential

$$u(r) = \begin{cases} \infty & r \leq \sigma \\ -\varepsilon & \sigma < r \leq \lambda\sigma \\ 0 & r > \lambda\sigma \end{cases}$$

where σ is the molecular diameter, ϵ and λ are the depth and range of the potential, respectively.

This fluid is in the presence of uniform walls, which exerts attractive forces on the particles. The molecule–wall interaction $U(z)$ is modeled by a square-well potential and as a function of the distance z from the wall:

$$U(z) = \begin{cases} \infty & z \leq \frac{\sigma}{2} \\ -\varepsilon_{\mathrm{W}} & \frac{\sigma}{2} < z \leq \lambda_{\mathrm{W}}\sigma \\ 0 & z > \lambda_{\mathrm{W}}\sigma \end{cases}$$

where σ, is the molecular diameter, and ϵ_{W} and λ_{W} are the depth and range of the potential of the wall–molecule potential.

DETAILS OF THE SIMULATION TECHNIQUE

The Gibbs ensemble simulation technique applied to confined systems [1] considers two simulation boxes, one for the bulk fluid and the other one for the confined fluid. Two types of movements were done:

(a) independent displacements of molecules in both boxes,

(b) interchange of molecules between boxes, keeping the total number of molecules constant.

We considered 1728 molecules. The initial configuration in each box consists of N/2 particles in an FCC arrangement. Periodic boundary conditions and minimum image convention were applied in the three x–y–z directions for the bulk, and for the confined fluid only in the in x–y directions [27,28].

The simulation was performed in cycles. Each cycle consists of a certain number of movements of type (a) in each box and a certain number of interchange of particles of type (b) at random. We considered 40,000 cycles in order to equilibrate and averages were taken over other 40,000 cycles. The maximum molecular displacement was adjusted in order to guarantee an acceptance rate of 40% in the translation movements.

The Gibbs ensemble simulation technique guarantees that the chemical potential are equal in both phases. This type of simulation does not require the knowledge of the values of this thermodynamic property in each phase in order to obtain the coexistence densities. Nevertheless, in order to assure that the system reaches the equilibrium, the chemical potential in each phase can be calculated using the Test Particle Insertion Method (TPI) [28,29] that uses part of the data generated in the Gibbs ensemble simulation. Since the TPI method is adequate only for not too dense fluids, for those states in which the fluid coexistence densities were

TABLE I Simulation results for a SW fluid confined between hard walls

λ	T^*	ρ^*_α	U^*_α	μ^*_α	ρ^*_β	U^*_β	μ^*_β
1.25	1.5	0.215(6)	− 0.80(3)	− 5.9	0.215(7)	− 0.84(3)	− 5.8
		0.384(10)	− 1.47(4)	− 5.2	0.384(11)	− 1.53(4)	− 5.3
		0.537(10)	− 2.12(4)	− 5.3	0.533(12)	− 2.22(5)	− 5.6
		0.821(26)	− 3.59(3)	− 6.9	0.794(38)	− 3.72(5)	− 7.5
	2.0	0.215(11)	− 0.71(3)	− 7.3	0.215(10)	− 0.75(3)	− 7.4
		0.386(13)	− 1.35(4)	− 6.1	0.388(12)	− 1.41(4)	− 6.3
		0.541(16)	− 2.01(4)	− 5.9	0.523(20)	− 2.09(4)	− 6.2
		0.755(33)	− 3.11(3)	− 6.7	0.729(46)	− 3.22(4)	− 7.2
1.50	1.5	0.205(11)	− 1.75(2)	− 7.3	0.224(9)	− 1.91(7)	− 7.3
		0.366(20)	− 2.86(8)	− 7.4	0.404(22)	− 3.14(8)	− 7.8
		0.527(17)	− 3.89(6)	− 8.2	0.547(22)	− 4.13(7)	− 9.1
		0.750(30)	− 5.28(3)	− 10.1	0.735(43)	− 5.52(4)	− 11.5
	2.0	0.211(8)	− 1.55(6)	− 8.7	0.218(6)	− 1.65(5)	− 8.8
		0.379(16)	− 2.68(6)	− 8.4	0.389(17)	− 2.85(5)	− 8.7
		0.535(8)	− 3.73(5)	− 9.0	0.537(11)	− 3.94(6)	− 9.7
		0.753(31)	− 5.18(3)	− 10.6	0.731(44)	− 5.39(5)	− 11.6
	3.0	0.214(10)	− 1.40(5)	− 11.6	0.216(9)	− 1.47(4)	− 11.9
		0.464(11)	− 3.08(5)	− 10.2	0.459(12)	− 3.22(6)	− 10.7
		0.613(21)	− 4.12(4)	− 10.6	0.600(28)	− 4.31(5)	− 11.3
		0.755(8)	− 5.07(3)	− 11.2	0.728(11)	− 5.28(5)	− 11.2

[a] The indexes α and β denote the confined fluid and the bulk fluid, respectively. The numbers in parentheses indicate the uncertainty in units of the last decimal digits. For example, 0.215(6) means 0.215 ± 0.006 and 0.613(21) means 0.613 ± 0.021.

high enough, the equilibrium criteria of observing the equality of the chemical potentials was complemented with the graphical analysis proposed by Frenkel and Smit [28].

We established a criterion in order to decide the optimum number of interchange of particles for each state. We observed that for not too dense fluids with an acceptance rate above 6% we obtained a better agreement for the chemical potentials in both boxes. For very dense fluids a higher number of attempts of interchange of particles is required.

All the simulation data were obtained by fixing the pore length $L_z = 15$ molecular diameters, a typical pore separation used in previous studies [17]. The reduced densities ρ^* were calculated by using a similar criterion than Vega *et al.* [10], i.e. using the ratio of the average number of molecules in a phase divided by the phase volume. In the case of the confined fluid this volume was taken equal to the $(L_z - \sigma) \times$ box length^2. We subtract σ from the pore length due to the nature of potential that we are considering. We changed the phase volume in the simulation in order to obtain data for different densities.

The averages of the thermodynamic properties were obtained dividing the simulation results in blocks of 25 cycles. The reported uncertainty corresponds to the average of the standard deviation over these blocks.

In order to calibrate our simulation program, we compared some of our results with available molecular dynamics simulation data reported in the literature [5,7,14,15] and we found a good agreement.

RESULTS

In Tables I–IV we present the simulation results for a SW fluid confined either between symmetrical walls or non-symmetrical walls. In each table the reduced density ρ^*, the reduced internal energy $U^* = U/N\epsilon$ and the reduced chemical potential $\mu^* = \mu/\epsilon$ for the confined (α) and bulk (β) fluids are presented at different reduced temperatures $T^* = kT/\epsilon$. We have selected three values for the reduced temperature: 1.5, 2.0 and 3.0 because these temperatures are supercritical for the bulk systems (SW) considered in

TABLE II Simulation results for a SW fluid confined between a SW wall and a hard-wall

T^*	ρ^*_α	U^*_α	μ^*_α	ρ^*_β	U^*_β	μ^*_β
1.50	0.207(12)	− 1.77(8)	− 7.3	0.222(10)	− 1.90(7)	− 7.4
	0.369(14)	− 2.88(8)	− 7.4	0.400(15)	− 3.11(8)	− 7.8
	0.529(22)	− 3.89(6)	− 8.3	0.544(28)	− 4.12(7)	− 9.1
	0.752(29)	− 5.31(4)	− 10.2	0.733(41)	− 5.51(5)	− 11.4
2.00	0.213(10)	− 1.57(6)	− 8.7	0.217(8)	− 1.64(5)	− 8.8
	0.380(9)	− 2.70(6)	− 8.4	0.388(9)	− 2.84(6)	− 8.7
	0.536(23)	− 3.75(5)	− 9.1	0.535(28)	− 3.93(6)	− 9.6
	0.753(37)	− 5.21(3)	− 10.7	0.731(37)	− 5.394(4)	− 11.6

[a] For these states we have chosen $\lambda = 1.5$, $\lambda_W = 0.70$ and $\varepsilon^*_W = 1.0$. See footnote to Table I for the notation used for the uncertainty estimates.

TABLE III Thermodynamic properties of a SW fluid confined between a left SW wall of variable depth ε_W^* and a right hard wall at $T^* = 1.5$

ε_W^*	ρ_α^*	U_α^*	μ_α^*	ρ_β^*	U_β^*	μ_β^*
0.25	0.206(10)	− 1.76(8)	− 7.2	0.223(8)	− 1.90(7)	− 7.4
	0.448(22)	− 3.39(7)	− 7.7	0.477(26)	− 3.63(8)	− 8.4
	0.679(16)	− 4.84(4)	− 9.5	0.674(22)	− 5.09(5)	− 10.6
0.5	0.206(11)	− 1.75(8)	− 7.4	0.223(10)	− 1.90(7)	− 7.3
	0.449(19)	− 3.39(7)	− 7.7	0.476(22)	− 3.63(8)	− 8.4
	0.681(19)	− 4.86(4)	− 9.5	0.671(26)	− 5.07(5)	− 10.7
1.5	0.209(11)	− 1.79(7)	− 7.3	0.220(10)	− 1.89(7)	− 7.4
	0.452(16)	− 3.40(7)	− 7.7	0.473(19)	− 3.60(8)	− 8.4
	0.682(16)	− 4.89(4)	− 9.6	0.669(21)	− 5.05(5)	− 10.6
2.0	0.212(10)	− 1.84(7)	− 7.4	0.218(9)	− 1.86(7)	− 7.2
	0.375(10)	− 2.92(8)	− 7.2	0.394(20)	− 3.07(8)	− 7.7
	0.533(30)	− 3.94(6)	− 9.0	0.540(20)	− 4.10(7)	− 9.0
	0.682(20)	− 4.92(4)	− 9.6	0.669(24)	− 5.04(6)	− 10.6

The parameters of the SW fluid are $\lambda = 1.5$ and $\lambda_W = 0.745$ for the SW wall. See footnote to Table I for the notation used for the uncertainty estimates.

this work. Different estimations [18,30–34] for the reduced critical temperatures of SW systems with ranges $\lambda = 1.25$ and 1.5 are within the intervals $0.764 \le T_c^* \le 0.788$ and $1.218 \le T_c^* \le 1.27$, respectively. The reported chemical potentials include the ideal gas contribution except for the term $T^* \ln \Lambda_d$. It is important to remark that the chemical potentials were calculated with a method that fails at high densities [29], so the data included in the tables at high densities must be regarded as a crude estimation.

SW Fluid Confined between Symmetrical Walls

In Table I the simulation data for the case of a SW fluid of variable range λ at different temperatures is presented. By using some of this data (without error bars, just to show the tendency of the central points), in Fig. 1 the adsorption isotherms expressed as the density in the bulk versus the density in the pore are exhibited for $\lambda = 1.5$ for $T^* = 1.5$, 2.0 and 3. For the three temperatures we observe a transition from a negative adsorption ($\rho_\alpha^* < \rho_\beta^*$) to a positive adsorption ($\rho_\alpha^* < \rho_\beta^*$) at a given density. This transition cannot be well observed from the figure for $T^* = 3$ but by looking at Table I one can see that $\rho_\alpha^* < \rho_\beta^*$ for the lower bulk density. The transition bulk density is lower for the system at the higher temperature, as expected, since an increment in temperature diminishes the cohesion of the bulk molecules.

In Fig. 2 we present the density profiles for two values for the SW range, $\lambda = 1.25$ and 1.5 for very close bulk densities at $T^* = 1.5$. We can see that for the larger value of λ the adsorption diminishes considerably, that is, the molecules prefer to remain in the bulk, an expected behavior, since a larger range of the SW potential means a greater attraction between the bulk molecules. Similar plots can be built for other densities and at other temperatures and the same effect of λ is observed.

In Fig. 3 the density profiles for a SW fluid ($\lambda = 1.25$) at $T^* = 2.0$ for different density values are shown. As the density is increased we observe an increase in the concentration of molecules near the walls. This result was expected, since by increasing the bulk density, for a given fixed volume, there are more available particles that can reach the walls. The same effect of the bulk density on the density profiles is observed for other temperatures and for other SW ranges. Notice that at higher densities the appearance of different layers can be observed.

Since the data presented in this work could be useful for future theoretical developments we also include an analysis of the behavior of the internal energy of

TABLE IV Thermodynamic properties of a SW fluid confined between a left SW wall of variable range λ_W and a right hard wall at $T^* = 1.5$

λ_ω	ρ_α^*	U_α^*	μ_α^*	ρ_β^*	U_β^*	μ_β^*
0.7	0.207(12)	− 1.77(8)	− 7.3	0.222(10)	− 1.90(7)	− 7.4
	0.369(14)	− 2.88(8)	− 7.4	0.400(15)	− 3.11(8)	− 7.8
	0.529(22)	− 3.89(6)	− 8.3	0.544(28)	− 4.12(7)	− 9.1
1.0	0.210(10)	− 1.79(8)	− 7.3	0.220(8)	− 1.88(7)	− 7.4
	0.452(19)	− 3.41(6)	− 7.8	0.472(22)	− 3.60(7)	− 8.3
	0.607(8)	− 4.41(5)	− 9.0	0.608(10)	− 4.60(6)	− 9.8
1.5	0.215(12)	− 1.88(8)	− 7.3	0.215(11)	− 1.84(7)	− 7.4
	0.454(18)	− 3.46(7)	− 7.9	0.470(21)	− 3.59(8)	− 8.3
	0.608(21)	− 4.45(5)	− 9.0	0.607(27)	− 4.58(6)	− 9.8
2.0	0.608(6)	− 4.49(5)	− 9.0	0.606(8)	− 4.58(6)	− 9.8

The parameters of the SW fluid are $\lambda = 1.5$ and $\varepsilon_W^* = 1.0$ for the SW wall. See footnote to Table I for the notation used for the uncertainty estimates.

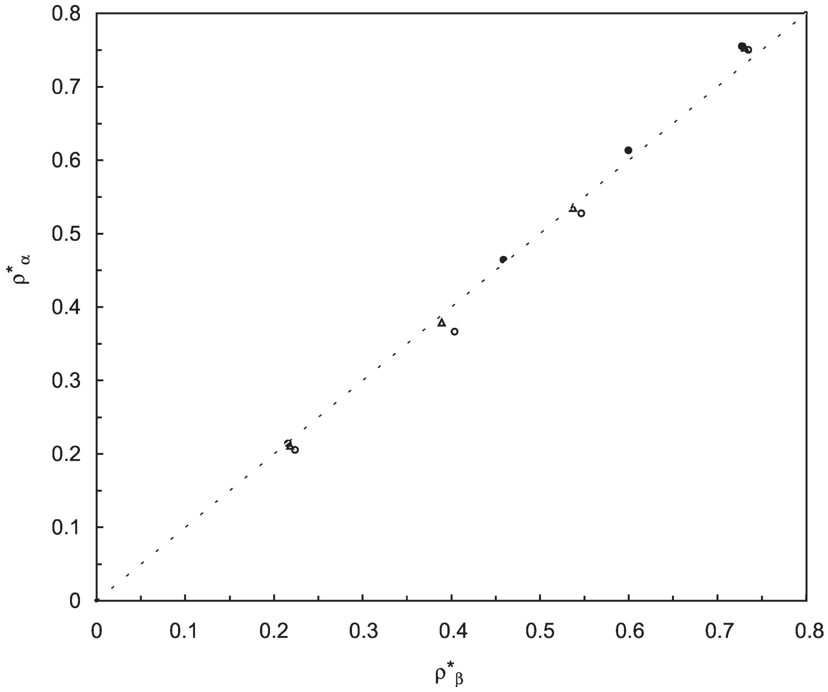

FIGURE 1 Adsorption isotherms for a SW fluid ($\lambda = 1.5$) confined between hard walls. The open circles are for $T^* = 1.5$, the open triangles are for $T^* = 2.0$ and the solid circles are for $T^* = 3.0$. The discontinuous line corresponds to the case the $\rho_\alpha^* = \rho_\beta^*$, and is included to distinguish between positive ($\rho_\alpha^* > \rho_\beta^*$) and negative ($\rho_\alpha^* > \rho_\beta^*$) adsorption.

the confined fluid as a function of the density, temperature and potentials parameters. By using the reported data in Table I, we observe that the internal energy of the confined fluid is sensitive to changes on the SW range, the temperature and the density. The internal energy of the confined fluid is always less negative than a non-confined fluid at similar thermodynamic conditions, a consequence of the global effect of the repulsive hard walls. The effect of varying the reduced bulk density on the reduced internal energy U_α^* for two different temperatures ($T^* = 1.5, 3.0$) for a SW fluid ($\lambda = 1.5$) confined between hard walls is

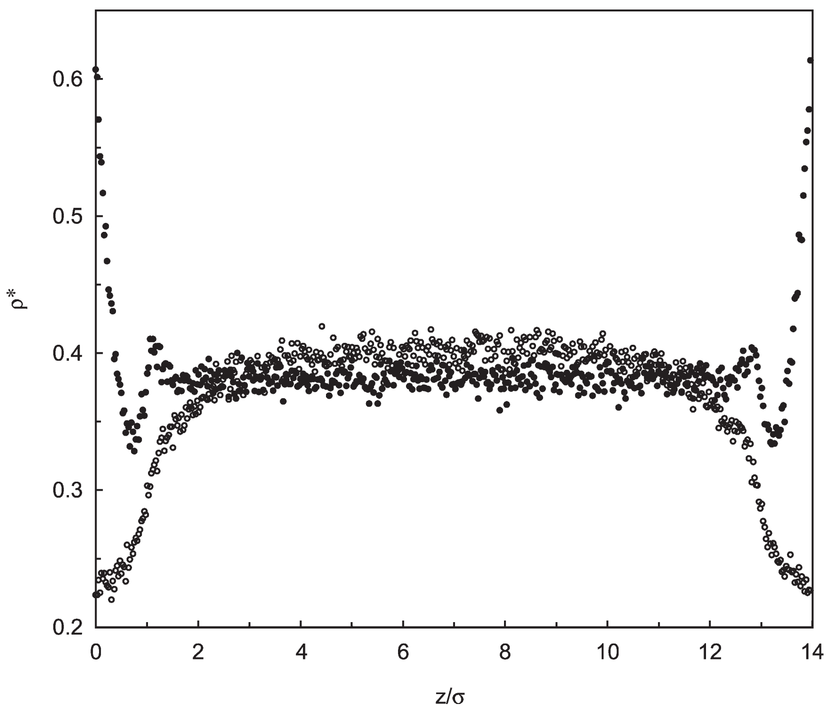

FIGURE 2 Density profiles for a confined SW fluid between hard walls at $T^* = 1.5$ and for different SW ranges and at very close bulk densities. The open circles represent the case $\lambda = 1.5$ at $\rho_\beta^* = 0.404$ and the solid circles represent the case $\lambda = 1.25$ at $\rho_\beta^* = 0.384$.

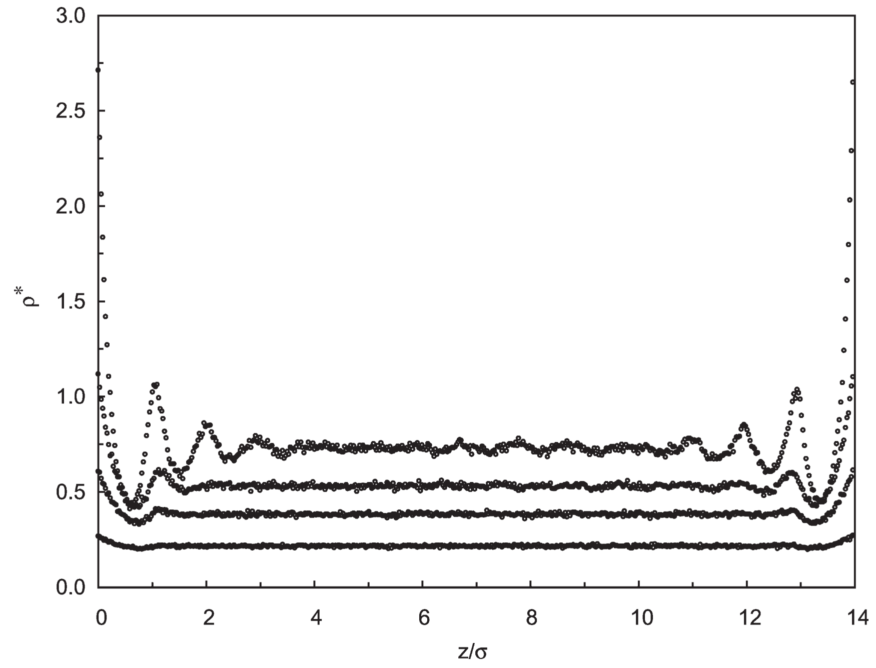

FIGURE 3 Density profiles for a SW fluid ($\lambda = 1.25$) confined between hard walls at $T^* = 2.0$ for different bulk densities $\rho^*_\beta = 0.215, 0.388, 0.523$ and 0.729. In the figure the series of points appear in ascendant order, i.e. the upper series corresponds to the higher density.

exhibited in Fig. 4. As can be seen from the figure an increase in the bulk density implies a more negative value of U^*_α for both temperatures. For a fixed density and a fixed λ, as the temperature is increased the internal energy becomes less negative whereas for a fixed temperature and a fixed λ the energy decreases by increasing the density. Also for fixed values of the density and temperature the internal energy becomes more negative when λ is increased. The explanation of effect of these parameters on the internal energy is the same than for a non-confined SW fluid.

SW Fluid Confined between Non-symmetrical Walls

In Table II, simulation results for a SW fluid ($\lambda = 1.5$) confined between non-symmetrical walls: a left SW wall ($\lambda_W = 0.7$, $\varepsilon^*_W = \varepsilon_W/\varepsilon = 1.0$) and a right hard

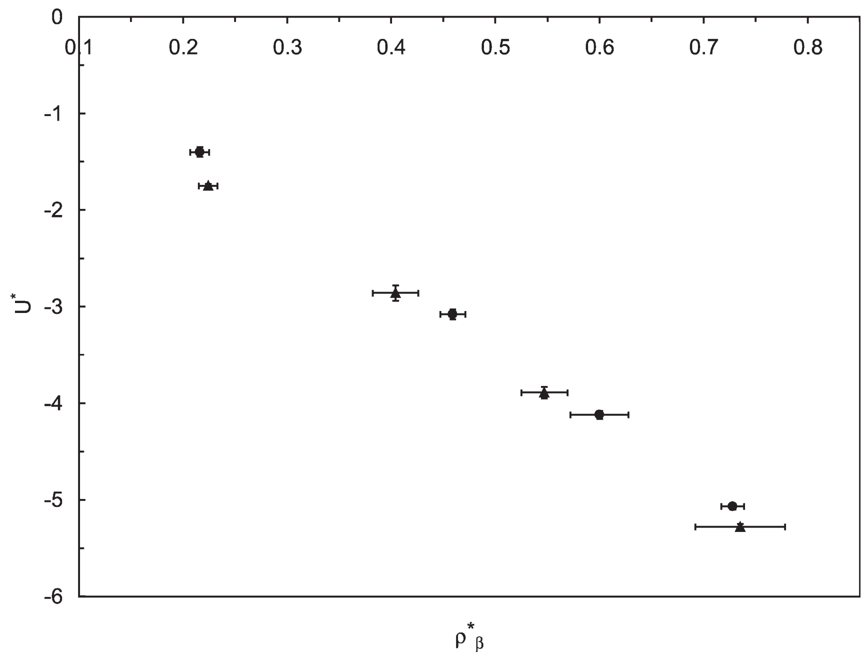

FIGURE 4 Reduced internal energy U^*_α as a function of the reduced bulk density ρ^*_β for a SW fluid of range $\lambda = 1.5$ confined between hard walls and for temperatures $T^* = 1.5$ (solid triangles) and $T^* = 3$ (solid circles).

wall are presented for two different temperatures and for different densities. In this case, the adsorption isotherms can be plotted as in the case of symmetrical walls but the information obtained is ambiguous since ρ_α represents the average density of the confined fluid and this type of plot gives a global information about the concentration of particles near both walls and not near a specific one. For instance, we can have a case of positive adsorption near one wall and a negative adsorption near the other, but on average $\rho_\alpha < \rho_\beta$, i.e. we have an effective negative adsorption. The same result can be obtained if we have a negative adsorption near both walls.

We observe that the symmetry of the density profiles is broken for all the cases of non-symmetrical walls considered in this work. We also observe that in contrast to systems confined between hard walls, the density profiles near the SW wall have a discontinuity at $z/\sigma = \lambda_W$ due to the discontinuity of the wall–molecule potential. Notice that in the case of a SW confined between hard walls, the discontinuity nature of the molecule–molecule potential does not induce a discontinuous density profile. This is in agreement with the density profile observed in real fluids.

In Fig. 5, the density profiles for different values of the bulk density at $T^* = 1.5$ for $\lambda = 1.5$ are shown. By looking at the right wall, we can see that as the bulk density is increased, for a given temperature, the slope of the density profile at contact pass from a negative to a positive value, showing that an increase of the bulk density promotes the concentration of particles near the wall. By looking at similar figures for $T^* = 2$ and (not included in this work) one can notice that the density profiles are slightly modified and in these cases there is only a positive adsorption, for all the bulk densities considered. It is expected that there exists a lower temperature for which the three densities analyzed show a negative adsorption. In general, for a given density, the temperature regulates the transition from one type of adsorption to another. A similar conclusion concerning the effect of density and temperature on the density profile is observed for $\lambda = 1.25$, although the transition from negative to positive adsorption occurs at lower temperatures. Henderson and van Swol [2] observed similar results for a gas–liquid confined system.

In order to see in more detail the adsorption in the left SW wall in Fig. 6, we made a re-scaling on the z/σ axis of the Fig. 5. It can be seen that as the bulk density is increased the concentration of the molecules near this wall is also increased. We obtained similar conclusions concerning the effect of varying the density or the temperature on the density profile for the right wall, but since the wall–molecule potential has an attractive part the concentration of particles is always grater than near the hard wall at similar conditions.

The thermodynamic properties of a SW fluid ($\lambda = 1.5$), confined between a left SW wall of variable depth ε_W^* and range $\lambda_W = 0.745$ and a right hard wall at $T^* = 1.5$ for different densities are presented in

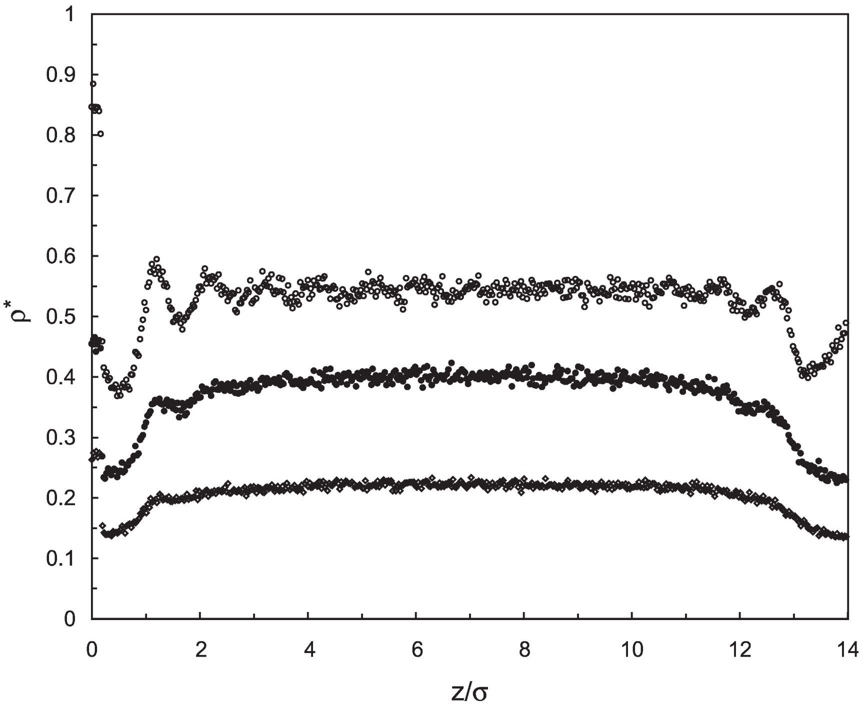

FIGURE 5 Density profiles for a SW fluid ($\lambda = 1.5$) confined between a left SW wall ($\lambda_W = 0.7$, $\varepsilon_W^* = 1.0$) and a right hard wall at $T^* = 1.5$, for different bulk densities $\rho_\beta^* = 0.222$, 0.400, 0.544. In the figure, the series of points appear in ascendant order, i.e. the upper series corresponds to the higher density.

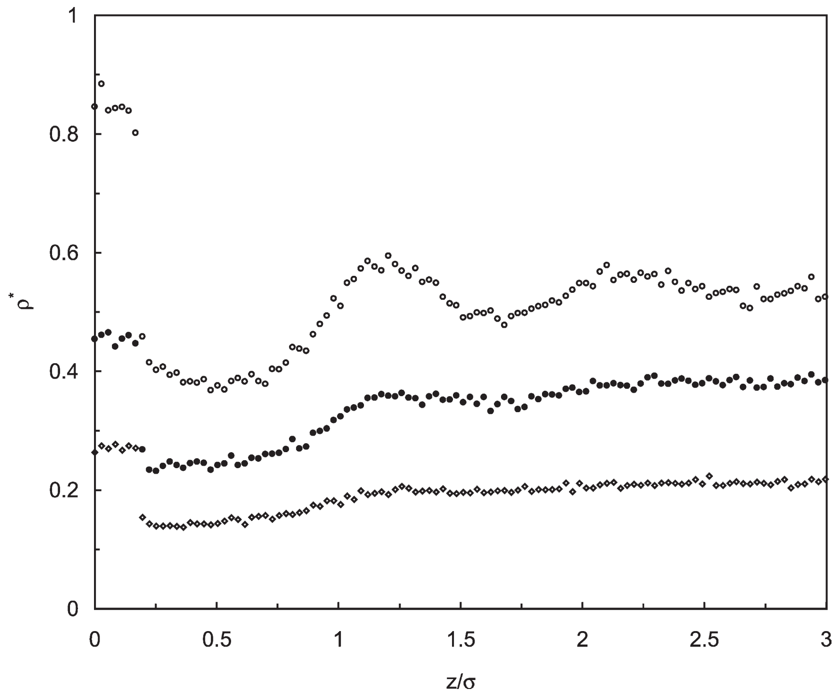

FIGURE 6 Figure 5 near the SW wall. See Fig. 5 for details.

Table III. In the Fig. 7 the effect of varying the parameter ε_W^* on the density profiles is shown for $\rho_\beta^* = 0.68$. As expected, since ε_W^* regulates the intensity of the wall–molecule attractive forces, an increment of λ_W increases the concentration of molecules near the SW wall. The effect of ε_W^* is more noticeable in the first monolayer due to the chosen values of λ_W in these cases.

The thermodynamic properties of a SW fluid ($\lambda = 1.5$, $\varepsilon = 1.0$) confined between a left SW wall ($\varepsilon_W^* = 1.0$) of variable range λ_W and a right hard wall at $T^* = 1.5$, are presented in Table IV. The effect of varying λ_W is shown in Fig. 8 for $\rho_\beta^* = 0.607$. A very similar qualitative behavior is observed for the three considered values of λ_W, nevertheless, in order to compare states at similar densities we show in this

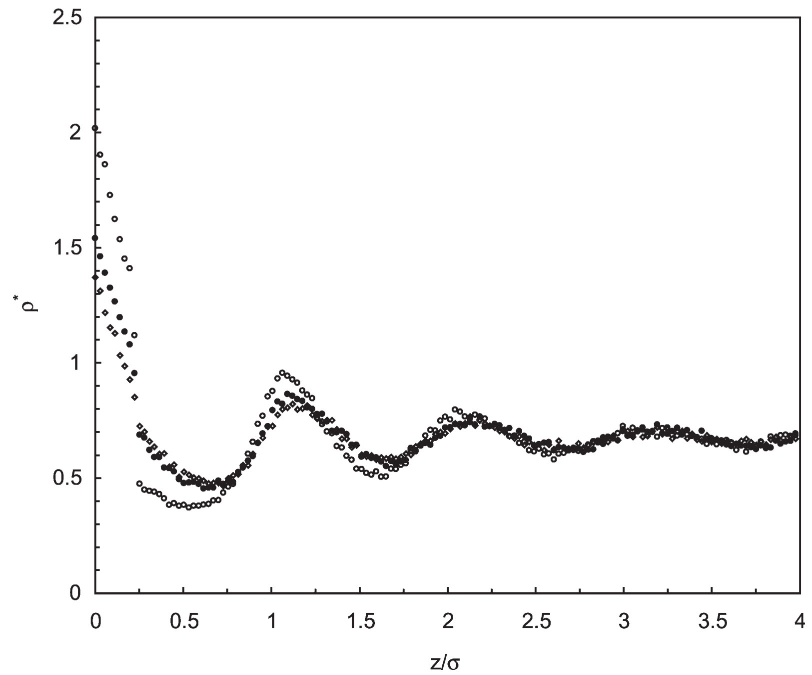

FIGURE 7 Density profiles for a SW fluid ($\lambda = 1.5$) confined between a left SW wall ($\lambda_W = 0.745$) and a right hard wall for different values of the wall depth at $T^* = 1.5$ and for $\rho_\beta^* = 0.68$. The open circles are for $\varepsilon_W^* = 1.5$, the solid circles are for $\varepsilon_W^* = 0.5$ and the open diamonds are for $\varepsilon_W^* = 0.25$.

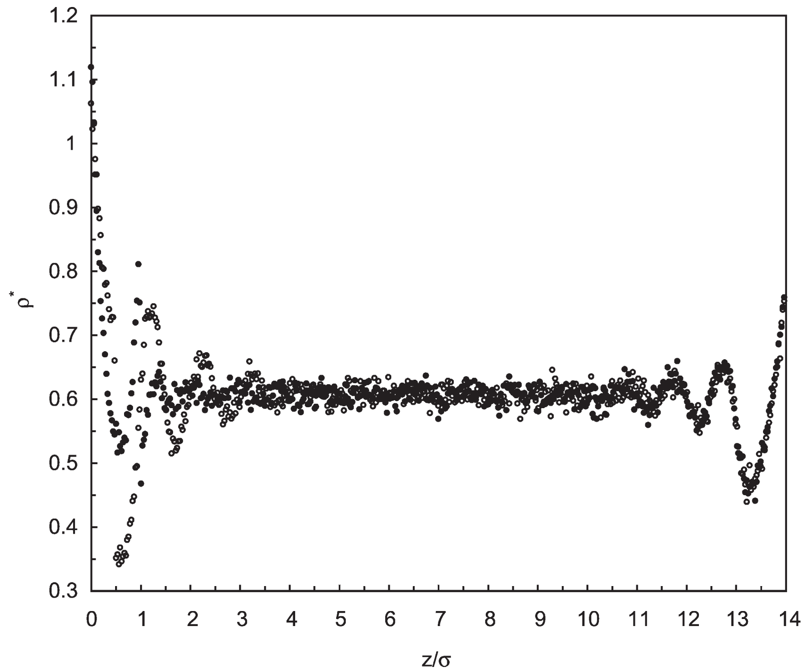

FIGURE 8 Density profiles for a SW fluid ($\lambda = 1.5$) confined between a left SW wall ($\epsilon_W = 1$) for different values of the wall SW range of at $T^* = 1.5$ for $\rho_\beta^* = 0.607$. The open circles are for the case $\lambda_W = 1.0$ and the solid circles are for $\lambda_W = 1.5$.

figure only the density profiles for two values of λ_W. Near the right hard wall the effect of λ_W is not appreciable, showing that for the pore length considered in this work, the two walls can be seen as independent.

In order to analyze the behavior near the left SW wall in Fig. 9 we made a closer caption of the Fig. 8 near this wall. A small difference in the density ρ^* at contact is observed for the two values of λ_W. The maximum corresponds to the higher value of λ_W. This behavior is expected since λ_W modulates the attractive part of the wall–molecule potential. By looking at other density profiles we observe that the influence of ε_W^* on the density at contact is more appreciable than that of λ_W for similar states. We also notice that the influence of λ_W is more relevant than

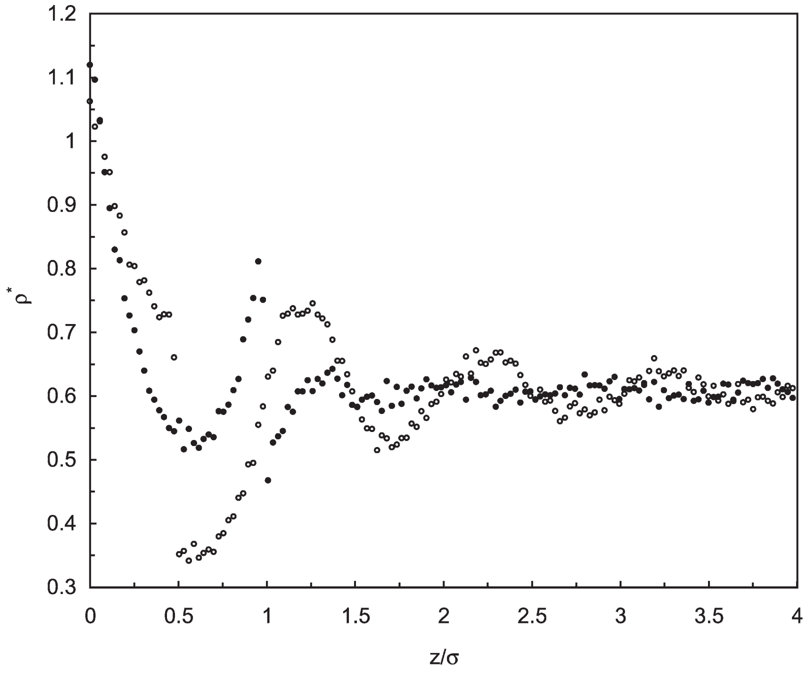

FIGURE 9 Figure 8 near the SW wall. See Fig. 8 for details.

ε_W^* in the vicinity of the wall. This explains the formation of multilayers as λ_W is decreased (see Fig. 9).

For the non-symmetrical case, the behavior of the internal energy of the confined fluid as a function of the density, temperature and potential parameters is reported in Table II. We observe that the internal energy of the confined fluid is always less negative than the bulk internal energy for all of the cases considered in this work. The net effect of the walls on U_α^* is repulsive for all of the selected cases. The attractive effect of the SW wall could be more important by choosing either a lower pore length or larger molecule–wall parameter potential.

By comparing the U_α^* (for a given λ, ρ_β^* and T^*) confined between symmetrical (Table I) and non-symmetrical walls (Table II) we also notice that the internal energy of the confined fluid is not very sensitive to the SW wall. Again, we expect that the effect of the SW wall could be more noticeable by choosing either a lower pore length or larger molecule–wall potential parameters.

The reduced internal energy U_α^* as a function of the SW wall potential depth ε_W^* for different bulk densities: $\rho_\beta^* = 0.22$, 0.47 and 0.67 is presented in Fig. 10. In this case $T^* = 1.5$, $\lambda = 1.5$ and $\lambda_W = 0.745$. For a fixed density, the effect of varying ε_W^* on U_α^* is negligible. It seems that because the pore length is large enough compared with λ_W and the walls are independent, ε_W^* only has an influence near the left wall and its effect is only noticeable on the structural properties of the system (i.e. density profile) and not in the internal energy, that is a global thermodynamic property. From the figure it also can be observed that the internal energy becomes more negative as the bulk density is increased for a fixed ε_W^*. More noticeable effects of ε_W^* could be obtained by considering either larger values of this parameter or larger values of λ_W as explained in the next paragraphs.

In Fig. 11 the reduced internal energy U_α^* as a function of the SW wall potential range λ_W for two density values at $T^* = 1.5$ and for $\lambda = 1.5$ and $\varepsilon_W^* = 1.0$ is presented. In general for a fixed density the effect of varying λ_W on U_α^* is small and becomes more noticeable for the lower density. Again, we expect that this effect becomes more important for larger values of the molecule–wall parameters and for a lower pore length.

For a fixed λ_W the internal energy becomes more negative as the bulk density is increased. A raise in the bulk density implies more interactions between the molecules in the bulk, resulting in a more negative value for the bulk internal energy that has a determining effect on the confined internal energy. This also explains the fact that the effect of λ_W on U_α^* is more important for lower densities.

By looking at the Tables III and IV one can see that the effect on U_α^* is more noticeable by varying λ_W than by varying ε_W^* by the same amount.

We have investigated the effect of the pore length for a confined fluid either between two SW walls and between a non-symmetrical wall (left SW wall and right hard wall) and as can be seen from the density profile shown in Fig. 12 for a pore length $L_z = 7\sigma$, there are no differences in the behavior near the left wall in the symmetrical and non-symmetrical cases, i.e. the walls can be also considered as independent for this pore length. Notice that the bulk properties

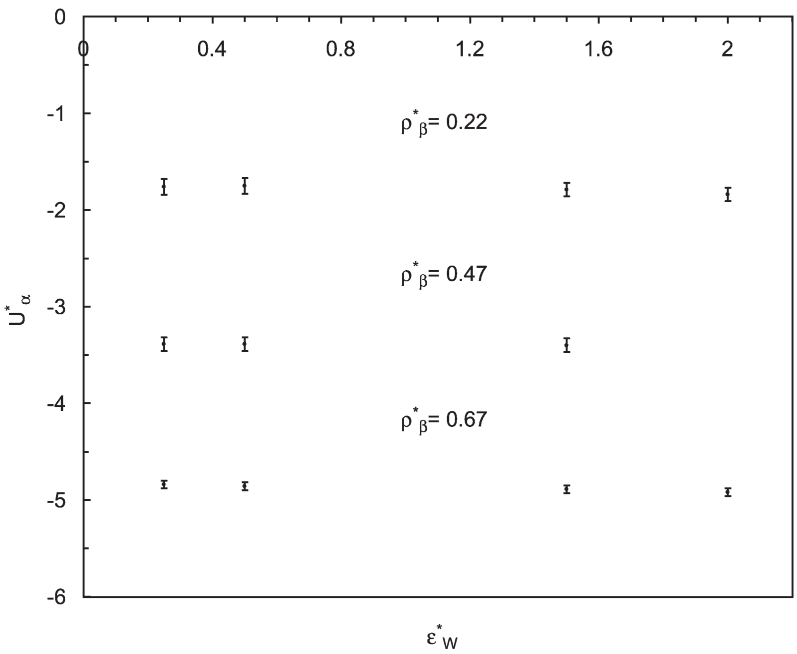

FIGURE 10 Reduced internal energy U_α^* as a function of the SW wall potential depth ε_W^* for three different bulk densities at $T^* = 1.5$, and for $\lambda = 1.5$ and $\lambda_W = 0.745$. The simulated data series are labeled with their corresponding bulk density value.

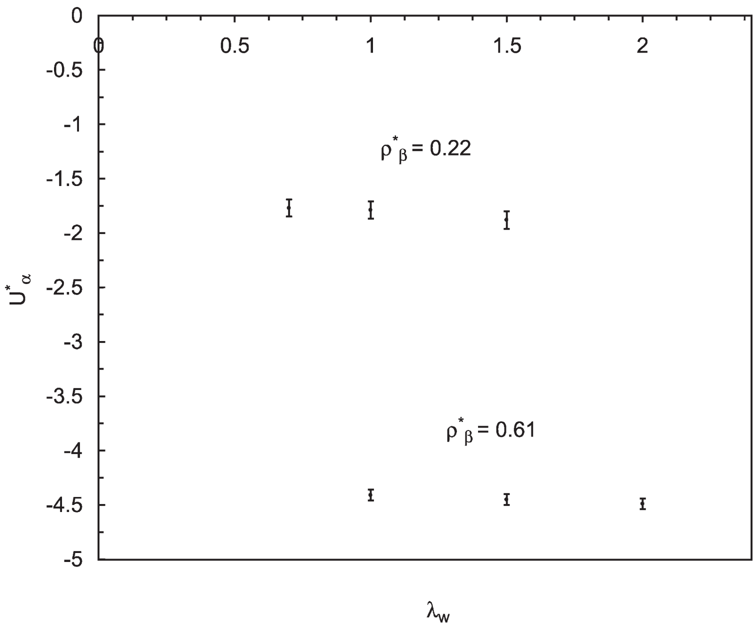

FIGURE 11 Reduced internal energy U^*_α as a function of the SW wall potential range λ_W for: two different bulk densities at $T^* = 1.5$ and for $\lambda = 1.5$ and $\varepsilon^*_W = 1.0$. The simulated data series are labeled with their corresponding bulk density value.

are similar for both types of confinements. In contrast to our results (for one single phase), Xiao and Rowlinson [17] found that for a hard SW system (in gas–liquid phase) confined between non-symmetrical walls this effect was important by using pore lengths of 12σ, 13σ and 15σ.

CONCLUSIONS

We have presented Gibbs ensemble simulation data for a SW confined fluid for different values of the potential parameters that characterize the molecule–molecule and molecule–wall interactions at supercritical states, for different temperatures, densities and for symmetrical and non-symmetrical walls.

After a general analysis of the simulation data, we conclude that the positive and negative adsorption can be induced by varying the potential parameters and also the temperature and the density. For instance, if one wants to increase the concentration of molecules close to the walls one needs to decrease λ or increase either T^* or ρ^*_β

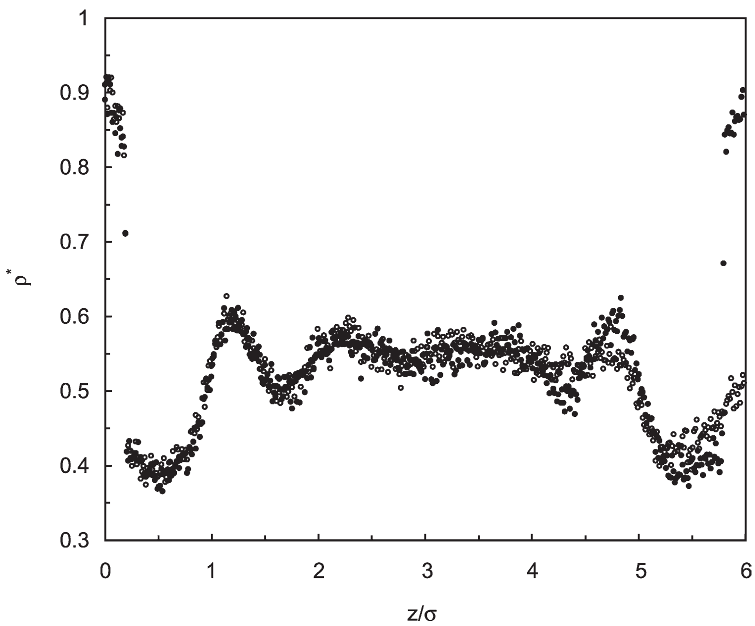

FIGURE 12 Density profile of a SW fluid confined between SW symmetrical walls (solid circles) and non-symmetrical walls: left SW wall and a right hard wall (open circles) for $T^* = 1.5$, $\lambda = 1.5$, $\varepsilon^*_W = 1.0$, $\lambda_W = 0.7$ and $\rho^*_\beta = 0.438$.

(keeping the rest of the parameters fixed), in the symmetrical case, but additionally, one can obtain this effect on the SW wall, by increasing any of the two SW wall parameters: λ_W, or ε_W^* We observed that the internal energy of the confined fluid is sensitive to changes on the temperature, the bulk density and λ. We also noticed that this thermodynamic property is less sensitive than the density profiles to changes on the molecule–wall potential parameters.

A rich variety of adsorption patterns were obtained with these simple models that can be useful in the development of new theories for confined systems.

A similar simulation study near the critical region and for different pore lengths is in progress.

Acknowledgements

L.A. del Pino is grateful to CONACyT for the financial support of his doctoral studies in México. A. Gil-Villegas acknowledges support from the Molecular Engineering Program (Instituto Mexicano del Petróleo, México).

References

[1] Panagiotopoulos, A.Z. (1987) "Adsorption and capillary condensation of fluid in cylindrical pores by Monte Carlo simulation in the Gibbs ensemble", *Mol. Phys.* **62**(3), 701–719.

[2] Henderson, J.R. and van Swol, F. (1985) "On the approach to complete wetting by gas at a liquid wall interface. Exact sum rules, fluctuation theory and the verification by computer simulation of the presence of the long range pair correlation at the wall", *Mol. Phys.* **56**(6), 1313–1356.

[3] van Swol, F. and Henderson, J.R. (1986) "Wetting at a fluid wall interface", *J. Chem. Soc. Faraday Trans.* **2**(82), 1685–1699.

[4] Bhethanabotla, V. and Steele, W. (1988) "Simulation of the thermodynamic properties of Kripton adsorbed on graphite at 100 K", *J. Phys. Chem.* **92**, 3285–3291.

[5] van Swol, F. and Henderson, J.R. (1989) "Wetting transitions at a fluid-wall interface: density—functional theory versus computer simulation", *Phys. Rev., A* **40**, 2567.

[6] Evans, R. (1992) Chapter 3, In: Henderson, D., ed, *Fundamentals of Inhomogeneous Fluids* (Dekker, New York).

[7] van Swol, F. and Henderson, J.R. (1991) "Wetting and drying transitions at a fluid–wall interface. Density-functional theory. II", *Phys. Rev., A* **43**(6), 2932–2942.

[8] del Río, F. and Gil-Villegas, A. (1991) "Monolayer adsorption of the square-well fluid of variable range", *J. Phys. Chem.* **95**(2), 787–792.

[9] Nigmeijer, M.J.P., Bruin, C., Bakker, A.F. and van Leeuwen, J.M.J. (1991) "Determination of the location and order of the drying transition with a molecular dynamic simulation", *Phys. Rev. B.* **44**(2), 834–837.

[10] Vega, L.F., Müller, E.A., Rull, L.F. and Gubbins, K.E. (1996) "Effect of surface activity sites on adsorption of associating chain molecules in pores: a Monte Carlo study", *Adsorption* **2**, 5968.

[11] Müller, E.A., Rull, L.F., Vega, L.F. and Gubbins, K.E. (1996) "Adsorption of water on activated carbons: a molecular simulation study", *J. Phys. Chem.* **100**, 1189–1196.

[12] Alejandre, J., Lozada-Cassou, M. and DeGrève, L. (1996) "Effect of pore geometry on a confined hard sphere fluid", *Mol. Phys.* **88**(5), 1317–1336.

[13] Olivares-Rivas, W., DeGrève, L., Henderson, D. and Quintana, J. (1997) "Grand canonical Monte Carlo and modified singlet integral equations for the density profile of a Yukawa fluid near a planar wall", *J. Chem. Phys.* **106**(19), 8160–8164.

[14] García, E. (1996) "Simulación de Adsorción de Fluidos" Master Thesis, Universidad de Guanajuato.

[15] Song, Y.J. and Kim, S.C. (1997) "Square-well confined in planar slits", *J. Chem. Phys.* **106**(9), 3821–3822.

[16] Smith, P., Lynden-Bell, R.M. and Smith, W. (2000) "The behavior of liquid alkanes near interfaces", *Mol. Phys.* **98**(4), 255–260.

[17] Xiao, C. and Rowlinson, J.S. (1994) "Drying transition at a square-well wall", *Mol. Phys.* **83**(6), 1299–1302.

[18] Schrader, M.E. (2000) "Negative gas solid adsorption and its influence on wettability", *J. Phys. Chem., B* **104**, 731.

[19] Fleming, III, P.E. and Brugman, R.J. (1987) "Towards a molecular equation of state for real materials", *AIChE J.* **33**, 729–740.

[20] Chang, J. and Sandler, S.I. (1994) "A completely analytic perturbation theory for square-well fluid of variable well width", *Mol. Phys.* **81**, 745–765.

[21] Fu, G.H. and Sandler, S.I. (1995) "A simplified SAFT equation of state for associating compounds and mixture", *Ind. Eng. Chem. Res.* **34**, 1897–1909.

[22] Gil-Villegas, A., del Río, F. and Benavides, A.L. (1996) "Deviation from corresponding-states behavior in the vapor–liquid equilibrium of the square-well fluid", *Fluid Phase Equillibria* **119**, 97–112.

[23] Gil-Villegas, A., Galindo, A., Whitehead, P.J., Mills, S.J., Jackson, G. and Burgess, A.N. (1997) "Statistical associating fluid theory for chain molecules with attractive potentials of variable range", *Chem. Phys.* **106**, 4168–4186.

[24] Vörtler, H.L. and Smith, W.R. (2000) "Computer simulation studies of a square-well fluid in a slit pore. Spreading pressure and vapor–liquid phase equilibria using the virtual parameter-variation method", *J. Chem. Phys.* **112**(11), 5168–5174.

[25] R. Evans, private communication (2002).

[26] Parry, A.O. and Evans, R. (1990) "Influence of wetting on phase equilibria: a novel mechanism for critical-point shifts in films", *Phys. Rev. Lett.* **64**(4), 439–442.

[27] Allen, M.P. and Tildesley, D. (1987) *Computer Simulation of Liquids* (Oxford Science Publications, New York).

[28] Frenkel, D. and Smit, B. (1996) *Understanding Molecular Simulation* (Academic Press Inc., San Diego CA).

[29] Widom, B. (1963) "Some topics in the theory of fluids statistical", *J. Chem. Phys.* **39**, 2808–2812.

[30] Vega, L., de Miguel, E., Rull, L.F., Jackson, G. and McLure, I. (1992) "Phase equilibria and critical behavior of square-well fluids of variable width by Gibbs ensemble Monte Carlo simulation", *J. Chem. Phys.* **96**, 2296–2305.

[31] Brillantov, N.V. and Valleau, J.P. (1998) "Thermodynamic scaling Monte Carlo study of liquid–gas transition in the square-well fluid", *J. Chem. Phys.* **108**, 1115–1122.

[32] Brillantov, N.V. and Valleau, J.P. (1998) "Effective Hamiltonian analyse of fluid criticality and application to the square-well fluid", *J. Chem. Phys.* **108**, 1123–1130.

[33] Elliott, J.R. and Hu, L. (1999) "Vapor–liquid equilibria of square-well spheres", *J. Chem. Phys.* **110**(6), 3043–3048.

[34] Orkoulas, G. and Panagiotopoulos, A.Z. (1998) "Phase behavior of restricted primitive model and square-well fluids from Monte Carlo simulation in the grand canonical ensemble", *J. Chem. Phys.* **110**, 1581–1590.